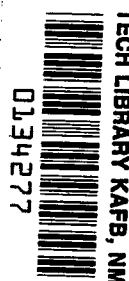


NASA Technical Paper 1079

LOAN COPY: RET
AFWL TECHNICAL
KIRTLAND AFB,

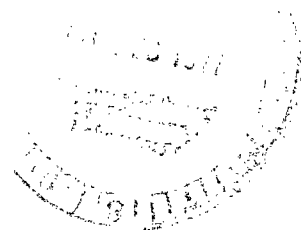


Effect of End-Ring Stiffness on Buckling of Pressure-Loaded Stiffened Conical Shells

Randall C. Davis and Jerry G. Williams

DECEMBER 1977

NASA





NASA Technical Paper 1079

Effect of End-Ring Stiffness on Buckling of Pressure-Loaded Stiffened Conical Shells

Randall C. Davis and Jerry G. Williams

Langley Research Center

Hampton, Virginia



National Aeronautics
and Space Administration

**Scientific and Technical
Information Office**

1977

SUMMARY

Buckling studies were conducted on truncated 120° conical shells having large end rings and many interior reinforcing rings that are typical of aeroshells used as spacecraft decelerators. An existing technique for casting epoxy models of such shells was used to produce cones that could be buckled repeatedly throughout a wide range of base-end-ring sizes. Changes in base-end-ring stiffness were accomplished by simply machining away a portion of the base ring between successive buckling tests. The ability to determine analytically the transition in buckling from extensional to inextensional behavior with decreasing base-ring size was verified by using buckling tests for comparison. Initial imperfection measurements from the test cones were included in the analytical model.

INTRODUCTION

The structural design of stiffened aerospace shell structures is often based on analyses that use a relatively simple beam or ring theory to account for discrete stiffeners. Such theories typically involve the area, inertia properties, and bending and twisting stiffnesses to account for the effect of the discrete stiffener on the behavior of the structure. (See refs. 1 to 4.) In a shell-of-revolution analysis, a severe test of the validity of such ring theories is the prediction of the buckling behavior of a shell with large end rings that provide an approximate simple support when attached to its edges. Published experimental data verifying this type of shell-stiffener combination are not adequate. In many cases, experimental data are for a configuration which has end rings that are deliberately oversized to avoid uncertainties associated with the ring behavior. (See refs. 5 to 9.) Thus, there is a need for tests with a wide range of end-ring sizes, including tests where the end-ring properties have a large effect on shell buckling behavior.

Such an investigation was begun in reference 10 by using small cast-epoxy conical shells in which the base-end-ring size was varied by machining material away from a solid cross-section base ring. Because buckling was not catastrophic, a large number of tests could be obtained from a single specimen for a wide range of base-ring sizes. However, the investigation was not completed in reference 10 because tensile failures occurred at the higher loads associated with the larger base-ring sizes. In the present investigation a technique for strengthening the cone was developed that allowed testing at all ring sizes. The purpose of the present paper is to report the results of the complete experimental investigation and to correlate these experimental results with analytical predictions of a shell-of-revolution analysis program in order to assess the adequacy of the ring theory.

SYMBOLS

The units used for physical quantities defined in this paper are given in the International System of Units (SI). Correlation between this system of units and U.S. Customary Units is given in reference 11. U.S. Customary Units were used in performing the calculations.

d	base-ring depth, cm (see fig. 1)
d_r	full size base-ring depth, cm (see fig. 1)
E	modulus of elasticity, N/m^2
I_x	ring moment of inertia about centroidal axis parallel to shell axis, cm^4
I_y	ring moment of inertia about centroidal axis normal to shell axis, cm^4
I_{xy}	ring cross product of inertia, cm^4
J	torsional constant, cm^4
n	number of full circumferential buckle waves
p	critical buckling pressure, N/m^2
p_r	critical buckling pressure of cone with full depth base ring, N/m^2
s	meridional coordinate with origin at support ring, cm
s_L	meridional length between base ring and support ring, cm
t	thickness, cm
u	displacement parallel to shell axis of revolution, cm
w	displacement of shell surface in radial direction, cm
\bar{w}	measured imperfection normal to shell surface, cm
x, y	Cartesian coordinates (see fig. 1)
\bar{x}, \bar{y}	location of ring centroid relative to ring attachment point on shell midsurface, cm
δ	imperfection amplitude, cm
ϵ_r	circumferential strain in rings
$(\epsilon_s)_i$	inside surface meridional strain

$(\epsilon_s)_o$	outside surface meridional strain
$(\epsilon_\theta)_i$	inside surface circumferential strain
$(\epsilon_\theta)_o$	outside surface circumferential strain
θ	circumferential coordinate, deg
μ	Poisson's ratio
ρ	density, g/m ³

Abbreviation:

LVDT linear voltage displacement transducer

SHELL GEOMETRY AND TEST PROCEDURE

The principal features of the conical shell can be seen in the cross-sectional drawing in figure 1. Computed cross-sectional properties for the various ring configurations in the shell structure are listed in table I and wall-thickness measurements are summarized in table II. Specimens A to E are the cones studied in reference 10; specimen F is identical to specimens A to E except for the addition of 12 equally spaced stringers added to reduce stresses in the vicinity of the support ring. Measured thicknesses are used in the analytical models employed in this paper. Material properties of the epoxy in the cones were determined from a series of standard coupon tests (ref. 12) and are summarized in figure 2. The material properties exhibited very little dependence on strain rate. Coupon tests were conducted over an 18-month period after casting and showed that the properties did not change with age. The fracture range shown is determined by plotting the highest and lowest fracture strains found for the test specimens.

The test apparatus shown in figures 3 and 4, described in detail in reference 10, was used to apply the external pressure to the cones. The entire pressure load was reacted at the support ring as indicated in figure 1. The membrane seal at the base ring shown in figure 3 causes a small axial reaction which was included in the analysis. For the buckling tests, displacements normal to the shell surface were measured by using LVDT's (linear voltage displacement transducer) positioned at eight circumferential locations. These displacement measurements were used to determine the circumferential mode shape of the buckle pattern. The circumferential position of maximum displacement was also noted for use in a repeat test. In the repeat test, the LVDT's were arranged on a meridional line through the position of maximum displacement to determine the meridional mode shape of the buckle pattern.

ANALYSIS PROCEDURE

In order to study various base-ring sizes, the cones were analyzed by using the BOSOR⁴ shell of revolution code described in reference 1. The

analytical model was based on the cross section shown in figure 1. The discrete rings were numbered 1 to 12, with the support ring numbered 1 and the base ring numbered 12. All 12 ring areas in the cross section are shaded, and the cross-hatched area on the base ring represents material removed by machining. The buckling loads for the various base-ring sizes were computed by using the option for bifurcation from a nonlinear prebuckling stress state in BØSØR4. In order to save computation time and costs, however, the buckling solutions used to study buckling boundary conditions and effects of model imperfections were computed by using bifurcation from a linear prebuckling stress state. Results for the static stress and strain analysis include nonlinear effects.

ANALYSIS AND TEST RESULTS

Strain Analysis

Comparisons of experimental strains with static stress analysis results are presented in figures 5 to 7. The experimental results are from reference 10 for a cone with a full depth base ring, without meridional stiffening subjected to an external pressure loading that was about half of its bifurcation buckling load. The theoretical results are for the cone with and without stringers and show the effect that meridional stiffeners have on the strains. The overall agreement between theoretical and experimental strains is considered to be good. Despite the large variations shown in figure 5 of the meridional strain with meridional location s/s_L caused by the internal stiffening rings, the analytical strains on the outside surface are within 23 percent of experiment, with the maximum difference occurring near s/s_L of 0.25. The agreement with experiment for the analytically computed circumferential strains is very good, as shown in figure 6(a). The analytical strains are within 15 percent of the experimental values, with the maximum deviation occurring near $s/s_L = 0.85$. Two distinct experimental strain values are shown in figure 6(a), at $s/s_L = 0.52$ and 0.8 where two strain gages were placed at different circumferential locations. The difference between the two strains gives some indication of the variation in experimental strain level with circumferential location. The small difference observed indicates that the cones were uniform castings of good quality.

In order to compare strains in the 12 rings, as shown in figure 7, the analytical strains on the surface of the rings at the strain-gage locations must include the strain induced by twisting of the ring. Strain gages at two different locations on the support ring gave the two strain values shown at $s/s_L = 0$ for this ring. Analytical strains at these two locations are shown for comparison. The agreement between analysis and experiment is good, with a maximum discrepancy of 25 percent occurring in the support-ring strains.

Effect of Meridional Stringers

An inspection of figure 5(b) shows a meridional tensile strain approaching 0.01 on the inside surface of the cone in the region between $s/s_L = 0.09$ and $s/s_L = 0$. The meridional strains at a pressure loading of 20.5 kN/m^2 in this highly strained region, when extrapolated to the 45 kN/m^2 buckling pressure

expected for this cone with a full base ring, will extend into the fracture range determined for the material. (See fig. 2.) Thus the fracture failures in the tests of reference 10, like the one shown in figure 3, were a consequence of high tensile strains induced on the inside surface of the cones near the support ring.

For the purpose of reducing the strains in the highly strained area near the support ring to the same level as the other meridional strains in the cone, various stringer geometries were studied in the analytical model. As shown in figure 1, the selected meridional stiffener design consists of 12 stringers equally spaced around the circumference. The stringer width is a constant 0.38 cm, but the stringer depth tapers from 0.38 cm at the support ring to 0 cm at ring 4. The casting mold used in reference 10 was modified to produce the selected stringer design in a test specimen.

The stringers added 0.2 percent to the computed mass of the shell but lowered the meridional strain near the support ring by almost a factor of three, as can be seen in figure 5. The strains shown by the dashed curve in figure 5 are shell surface strains computed from stress resultants for a smeared stringer analysis.

Results of Buckling Tests

As the load increases, normal displacements measured by the LVDT's show a nearly uniform increase in deflection all around the shell up to pressures near the buckling pressure. Near buckling, as the buckle shape begins to develop, the inward displacements begin to increase disproportionately with load while outward displacements start to decrease. Plots of the displacements at different values of pressure, as shown in figure 8, illustrate the development of the mode shape with load. Those LVDT's which show a reversal are used to determine the buckling pressure. The experimental-bifurcation buckling pressure, for the purposes of this paper, is defined as that pressure at which the first of these LVDT displacement curves begin to decrease with increasing pressure. The pressure marked "experimental bifurcation" in figure 9 corresponds to the pressure for the LVDT curve on the extreme right which first gave evidence of a reduction in deflection or reversal. The results of the buckling tests are given in table III and include results from reference 10. The experimental and theoretical bifurcation pressures for the various base-ring configurations investigated are tabulated as well as the wave number of the buckle mode.

Shown in figure 10 are the buckling pressures for cones without stringers and shown in figure 11 are the results for a cone with stringers. The two segments of the buckling curves shown in these figures are the result of two buckling phenomena. (See ref. 13.) For base-ring depth ratios above 0.75, the critical buckle mode is six full waves ($n = 6$) of the extensional type shown in figure 12(a). The critical mode below 0.75 is three full waves of the inextensional type shown in figure 12(b). For the $n = 6$ mode, increases in base-ring size above $d/d_r = 0.75$ have very little effect on the buckling pressure. In fact, if the base ring were made infinitely stiff, the buckling pressure would be increased to only 50.5 N/m^2 , a 12-percent increase over the buckling pressure for $d/d_r = 1.0$.

By supporting the cone on the test fixture as shown in figure 3, only the axial displacement of the shell is restrained, thereby giving the prebuckling boundary constraint of $u = 0$ only at this edge. The large axial load from the cone, reacted by the fixed support, presses the support ring down to the support plane. Therefore, a larger counterload would be needed to lift the support ring off of the support. Since initial buckling only involves small forces, the buckling boundary condition $u = 0$ seems appropriate for analysis. This assumption is substantiated by the results presented in figure 13, in which it can be seen that the $u \neq 0$ buckling loads are considerably lower than the $u = 0$ buckling loads. It is the $u = 0$ analytical buckling loads that agree with experimental loads shown in figures 10 and 11. With $u = 0$, the buckling pressure for the $n = 2$ mode is driven up to pressures above the $n = 3$ mode which then becomes the lowest inextensional buckling mode for d/d_r from 0 to about 0.75. Resistance to radial motion, caused by friction and the large axial load, is considered to be negligible during buckling. The curve for $w = 0$ in figure 13 corresponds to infinite friction to radial motion. The case of infinite radial friction and no axial movement is represented by the composite curve $u = 0; w = 0$ in figure 13. The assertion that friction does not appreciably constrain the radial displacement during buckling is borne out by the fact that the experimental test points in figure 11 tend to follow the analysis curve for both load and mode number.

The agreement shown in figures 10 and 11 between experiment and analysis is considered to be good. For the cone without stringers, figure 10 shows that the test loads are higher than the analysis loads; for the cone with stringers, figure 11 shows that two of the test loads are higher than the analysis loads. The experimental data at $d/d_r = 0.67$ agrees well with the curve $n = 6$, but analysis predicts an $n = 3$ mode for this base-ring size. The usual experience in testing shells has been that considerable differences between theory and experiment have been observed. In reference 14 a knockdown factor of 0.75 is recommended for cones subject to pressure loading, based on the lower limit of experimental data for monocoque cones. This factor appears to be too severe for the current tests.

For the tests where extensional modes developed, the change in displacement pattern with increasing pressure was sudden and sharp. In tests where inextensional modes developed the displacement change began slowly and took a considerable increase in pressure for the mode to be fully developed. (See, for example, fig. 9). Where the displacement decrease was sudden, the bifurcation pressure was easily determined whereas for slow changes, such as shown in figure 9, the tangent point was not well defined.

The cones exhibited a plateau shown by the pressure labeled "experimental collapse" in figure 9. This plateau occurred nearly simultaneously for all the LVDT's in a test and was thus easily determined for most of the cones. For cones with inextensional buckling modes, this plateau occurred at the maximum pressure carried. For the cones with extensional modes, however, this plateau was merely an inflection point in the pressure displacement curve where considerable deflection was observed before the pressure continued to increase. The experimental collapse for cones which buckled in an inextensional mode occurred at pressures considerably higher than the experimental bifurcation pressures. (See fig. 9.) For the cones which buckled in an extensional mode,

the pressure for the plateau was only slightly higher than the experimental bifurcation pressure. Figure 12 is a comparison plot showing the shape of the extensional and inextensional modes as determined by analysis.

The effect of the stringers on the analytical buckling load was investigated by comparing the analytical curves shown in figures 10 and 11. The stringers have very little effect on the $n = 6$ buckling pressure near $d/d_r = 1.0$ where the stringers increase the pressure by 2 percent. For the $n = 3$ mode, the stringers increase the pressure from about 5 percent near $d/d_r = 0.75$ to about 25 percent near $d/d_r = 0$.

IMPERFECTIONS

The cones were measured after fabrication, as described in reference 10, to determine the magnitude and shape of any initial deviations from a perfect cone. The data revealed that all specimens had similar imperfections typical of the data shown in figure 14. The imperfections are nearly axisymmetric with a single half-wave shape in the meridional direction with a maximum amplitude between 0.5 and 0.6 of the shell-wall thickness. For an axisymmetric half-sine-wave imperfection in the analytical model, the maximum amplitude of the measured shape and the length of the shell meridian were used as the amplitude and half-wave length, respectively.

The effect of varying the amplitude of a half-sine-wave imperfection on the linear bifurcation buckling pressure for the cone with stringers is shown in figure 15. For comparison purposes, the buckling pressures are normalized with p_r , which is the $n = 6$ buckling pressure for a cone with no imperfections and $d/d_r = 1$. In general, it can be seen that the buckling pressures are fairly insensitive to axisymmetric imperfections. The imperfection reduces the $n = 6$ analytical load by 2 percent whereas the $n = 3$ mode is almost totally insensitive to the imperfections up to large amplitudes. The $n = 5$ mode was found to be more sensitive than any of the other modes. Results in table III for $d/d_r = 0.33$ and 0.68 indicate that imperfections may have influenced the mode wave numbers; however, no firm explanation for the differences in the buckling wave numbers between test and theory shown in table III was established by considering axisymmetric imperfections with linear theory. The fact that some modes were found to be more imperfection sensitive than others suggests that more accurate imperfection measurements and modeling may be needed to establish any connection between imperfections and shifting wave numbers.

CONCLUSIONS

Results have been presented from an investigation of the effect of base-end-ring stiffness on the buckling of stiffened conical shells loaded by external pressure. Theoretical calculations were made for stress, buckling, and the effect of axisymmetric imperfections by using a shell-of-revolution analysis with discrete ring theory. Predicted and measured strains during pressure loading were in good agreement. Buckling predictions for both extensional and inextensional modes were in very good agreement with test data.

Theoretical predictions of the effects of measured imperfections using linear theory confirmed the fact that imperfection effects were small but failed to explain mode-shape differences. Based on these comparisons, it is concluded that the adequacy of the theory to predict the buckling behavior of conical shells over a wide range of base-end ring sizes has been demonstrated.

Langley Research Center
National Aeronautics and Space Administration
Hampton, VA 23665
October 27, 1977

REFERENCES

1. Bushnell, David: Stress, Stability, and Vibration of Complex Branched Shells of Revolution: Analysis and User's Manual for B~~Ø~~S~~Ø~~R4. NASA CR-2116, 1972.
2. Cohen, Gerald A.: Computer Analysis of Ring-Stiffened Shells of Revolution. NASA CR-2085, 1973.
3. Heard, Walter L., Jr.; Anderson, Melvin S.; and Chen, Ming M.: Computer Program for Structural Analysis of Layered Orthotropic Ring-Stiffened Shells of Revolution (SALORS) - Linear Stress Analysis Option. NASA TN D-7179, 1973.
4. Svalbonas, V.: Numerical Analysis of Stiffened Shells of Revolution - Volume I of VII. NASA CR-2273, Vol. I, 1973.
5. Heard, Walter L., Jr.; Anderson, Melvin S.; Anderson, James Kent; and Card, Michael F.: Design, Analysis, and Tests of a Structural Prototype Viking Aeroshell. J. Spacecr. & Rockets, vol. 10, no. 1, Jan. 1973, pp. 56-65.
6. Anderson, James Kent; and Davis, Randall C.: Buckling Tests of Two 4.6-Meter-Diameter, Magnesium Ring-Stiffened Conical Shells Loaded Under External Pressure. NASA TN D-7303, 1973.
7. Anderson, James Kent; and Davis, Randall C.: Buckling Tests of Three 4.6-Meter-Diameter Aluminum Honeycomb Sandwich Conical Shells Loaded Under External Pressure. NASA TN D-7935, 1975.
8. Cohen, Gerald A.; Foster, Richard M.; and Schafer, Everett M.: Analysis of Conceptual Designs for the Voyager Entry Capsule. Contract No. NAS 1-5554-1, Space & Re-Entry Systems Div., Philco-Ford Corp., [1968]. (Available as NASA CR-66580.)
9. Dixon, Sidney C.; Miserentino, Robert; and Hudson, M. Latrelle: Theoretical and Experimental Vibration and Buckling Results for Blunt Truncated Conical Shells With Ring-Supported Edges. NASA TN D-7003, 1970.
10. Williams, J. G.; and Davis, R. C.: Buckling Experiments on Stiffened Cast-Epoxy Conical Shells. J. Exp. Mech., vol. 15, no. 9, Sept. 1975, pp. 329-338.
11. Metric Practice Guide. E 380-72, American Soc. Testing & Mater., June 1972.
12. Plastics - General Test Methods; Nomenclature. Part 35 of 1977 Annual Book of ASTM Standards, c.1977.

13. Davis, Randall C.; and Cooper, P. A.: Interactive Design of Large End Rings on Stiffened Conical Shells Using Composites. Comput. & Struct., vol. 4, no. 3, May 1974, pp. 647-657.
14. Buckling of Thin-Walled Truncated Cones. NASA SP-8019, 1968.

2

TABLE I.- RING PROPERTIES

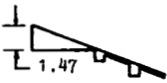

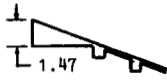
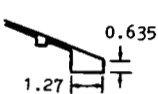
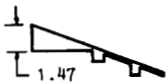
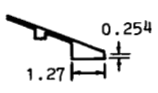
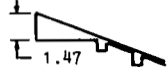

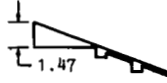

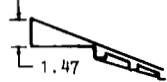
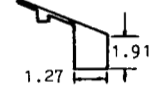
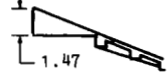
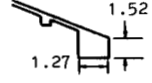
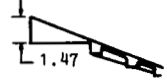
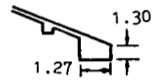
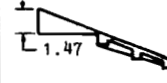
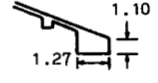
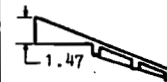
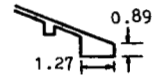
Property	Base ring with d/d_r of -								Interior rings	Support rings
	1.0	0.8	0.67	0.58	0.47	0.33	0.13	0		
Area, cm^2 . . .	2.885	2.401	2.079	1.863	1.595	1.272	0.788	0.466	0.1864	2.081
I_y , cm^4	0.3844	0.3187	0.2747	0.2451	0.2082	0.1633	0.0936	0.0417	0.002225	1.2658
I_x , cm^4	1.3049	0.7688	0.5099	0.3750	0.2447	0.1342	0.0419	0.0139	0.004132	0.3577
I_{xy} , cm^4 . . .	-0.11093	-0.08741	-0.07929	-0.07076	-0.06010	-0.04712	-0.02701	-0.01203	-0.000642	-0.4699
J , cm^4	1.0252	0.7642	0.5944	0.4849	0.3569	0.2200	0.0712	0.0211	0.004828	0.2890
\bar{y} , cm	-0.2222	-0.1924	-0.1724	-0.1590	-0.1423	-0.1219	-0.09024	-0.6669	-0.04535	0.08854
\bar{x} , cm	0.09315	0.09205	0.09106	0.09024	0.08886	0.08642	0.07906	-0.06563	-0.002205	-0.2631

TABLE II.- CONICAL-SHELL WALL-THICKNESS MEASUREMENTS

Conical-shell specimen	Maximum thickness, cm	Minimum thickness, cm	Mean thickness, cm (a)
A	0.104	0.099	0.102 (± 2.5)
B	.107	.098	.103 (± 4.4)
C	.106	.099	.103 (± 3.4)
D	.106	.099	.103 (± 3.4)
E	.108	.099	.104 (± 4.3)
F	.108	.101	.105 (± 3.6)

^aVariation is given as a percentage.

TABLE III.- ANALYTICAL AND EXPERIMENTAL RESULTS

Case	Specimen	Support-ring configuration (a)	Base-ring configuration (a)	Buckling pressure, kN/m^2		Number of circumferential waves		Base-ring depth ratio, d/d_r
				Experimental bifurcation	Analytical bifurcation	Experimental	Analytical	
1	A			(b)	41.4	(b)	6	1.0
2	B			16.1	13.0	4	3	0.33
3	C			8.96	7.91	3	3	0.13
4	D			6.76	6.48	3	3	0
5	E			6.76	6.48	3	3	0
6	F			42.1	42.2	6	6	1.0
7	F			41.4	41.6	6	6	0.80
8	F			40.4	33.9	5	3	0.68
9	F			28.3	27.3	3	3	0.58
10	F			19.9	20.4	3	3	0.47

^aDimensions are in centimeters.^bSpecimens fractured.

1

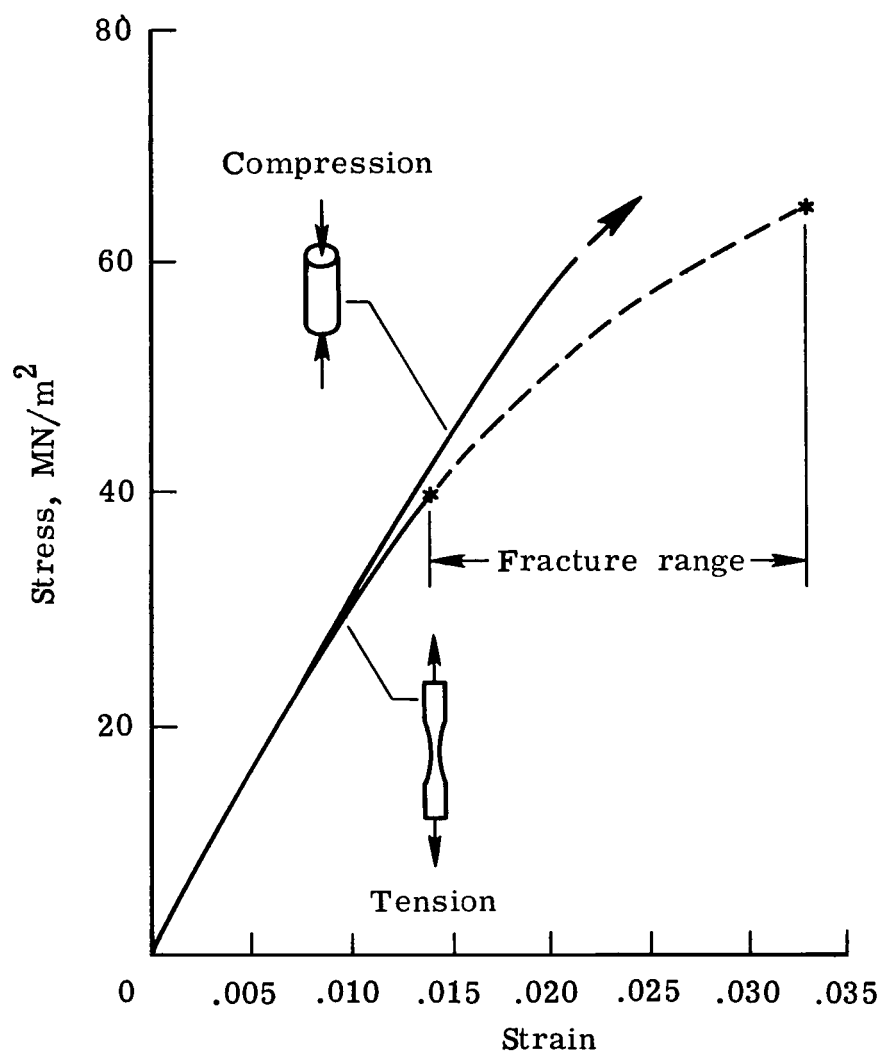
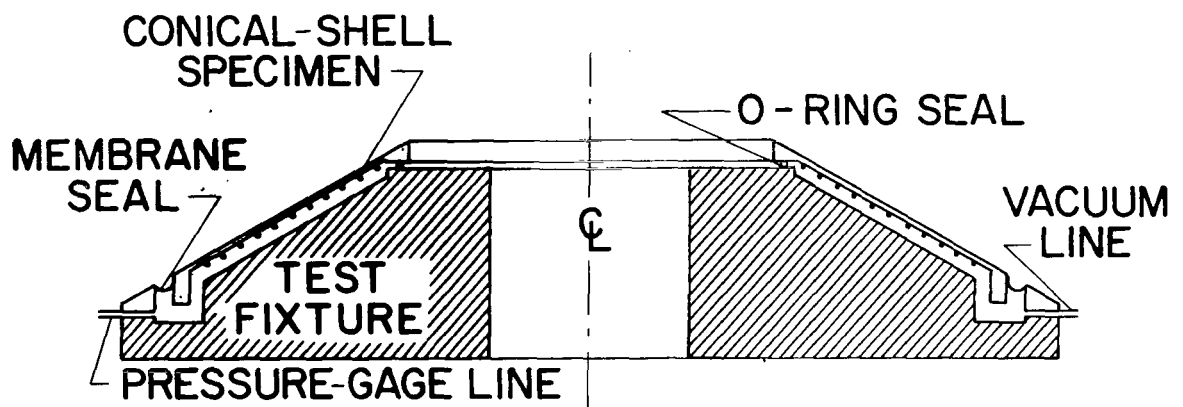
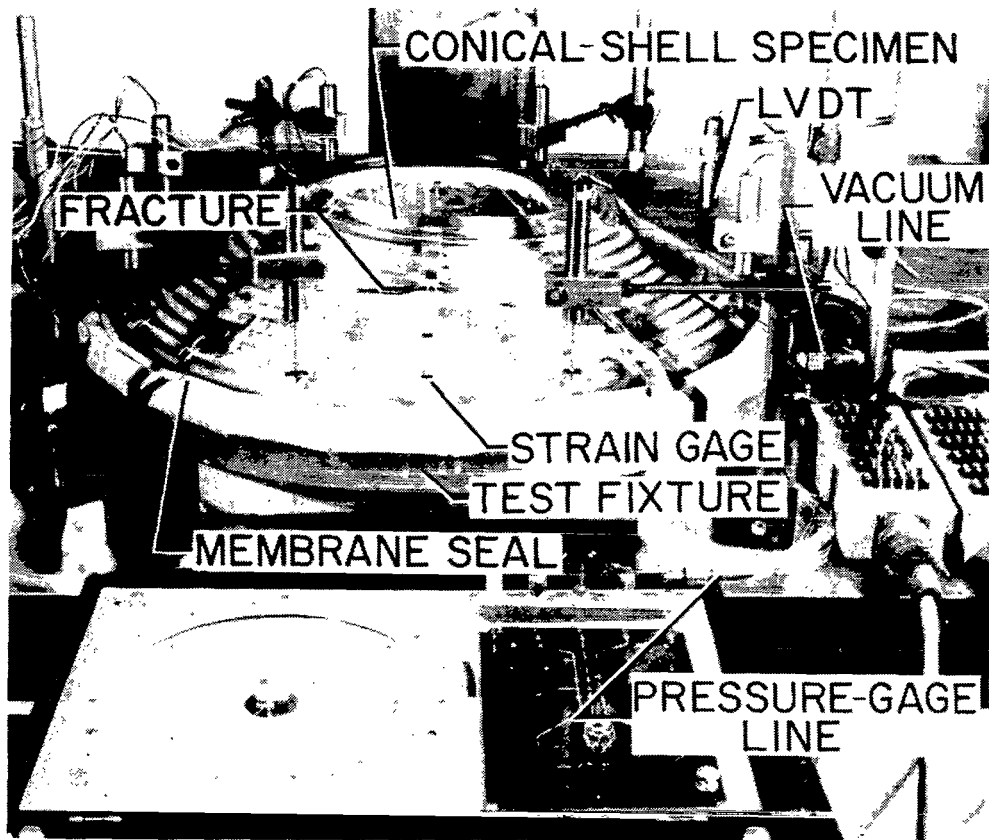


Figure 2.- Room-temperature stress-strain curves for the clear epoxy casting resin. $E = 3.00 \text{ GN/m}^2$; $\mu = 0.370$; $\rho = 1154 \text{ kg/m}^3$.



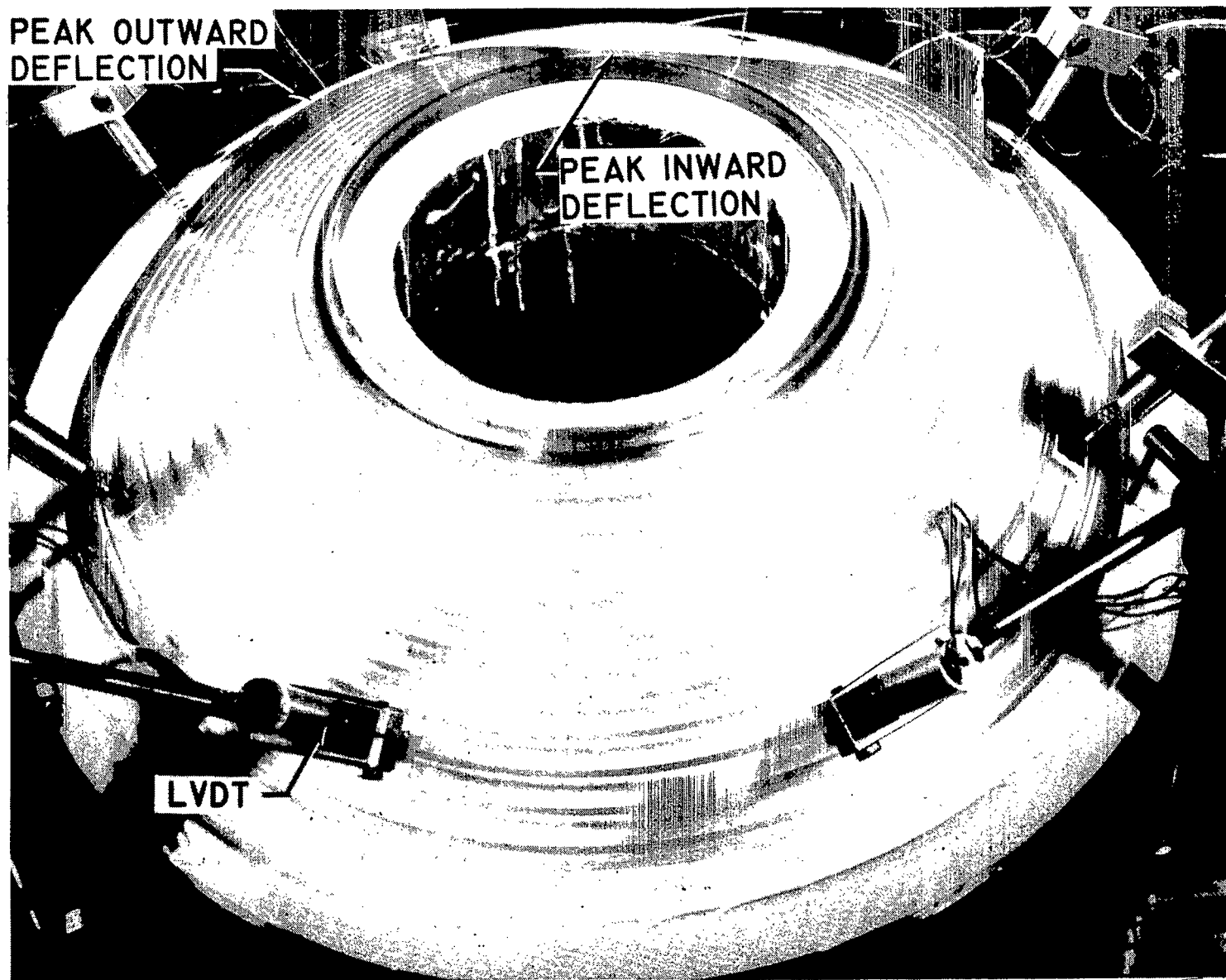
(a) Cone and test-fixture cross section.



(b) Test setup.

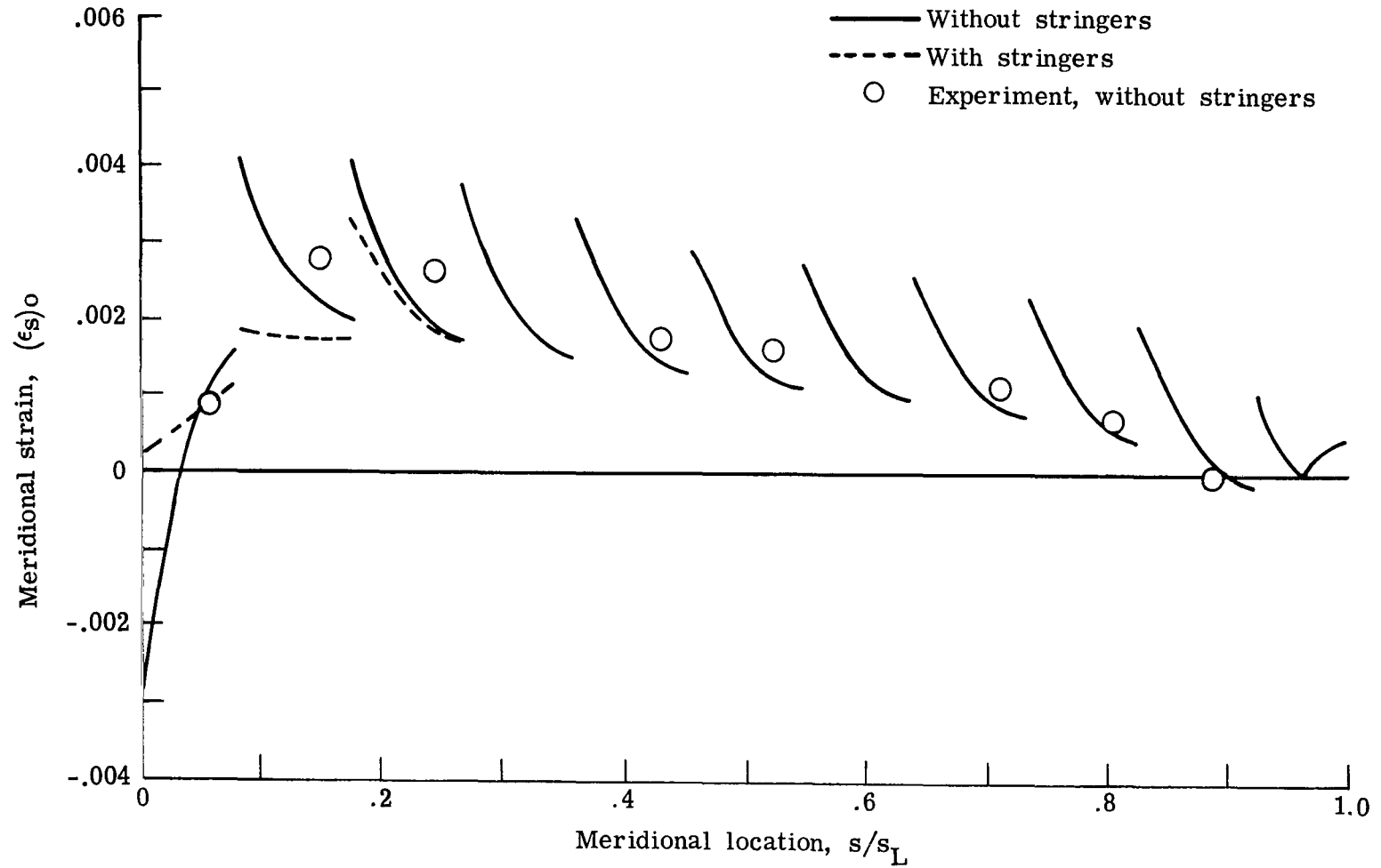
L-73-1485.1

Figure 3.- Experimental apparatus and schematic of cone in test fixture. Case 1.



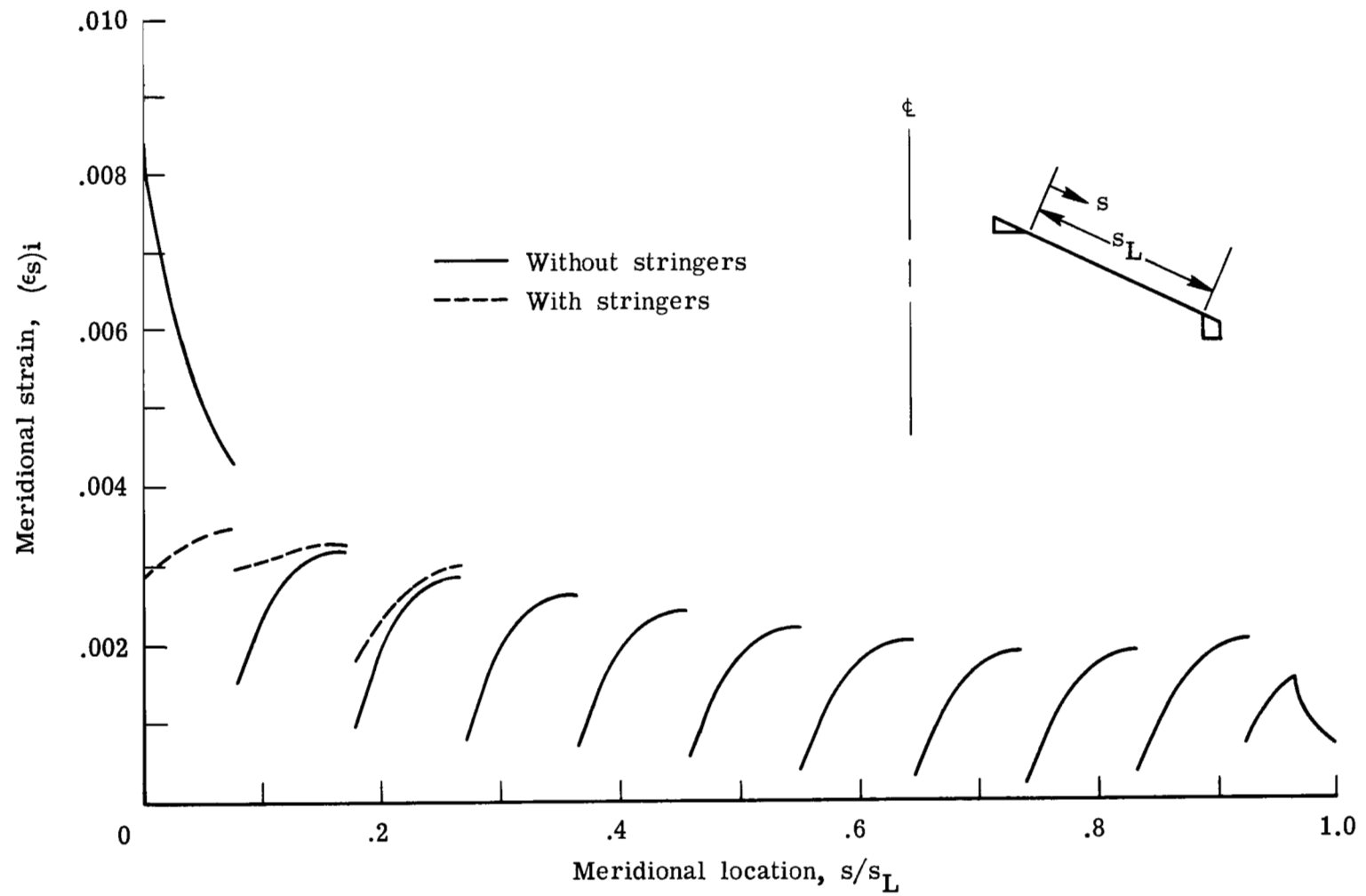
L-73-1709.1

Figure 4.- Buckled conical shell exhibiting three full circumferential waves. Case 3.



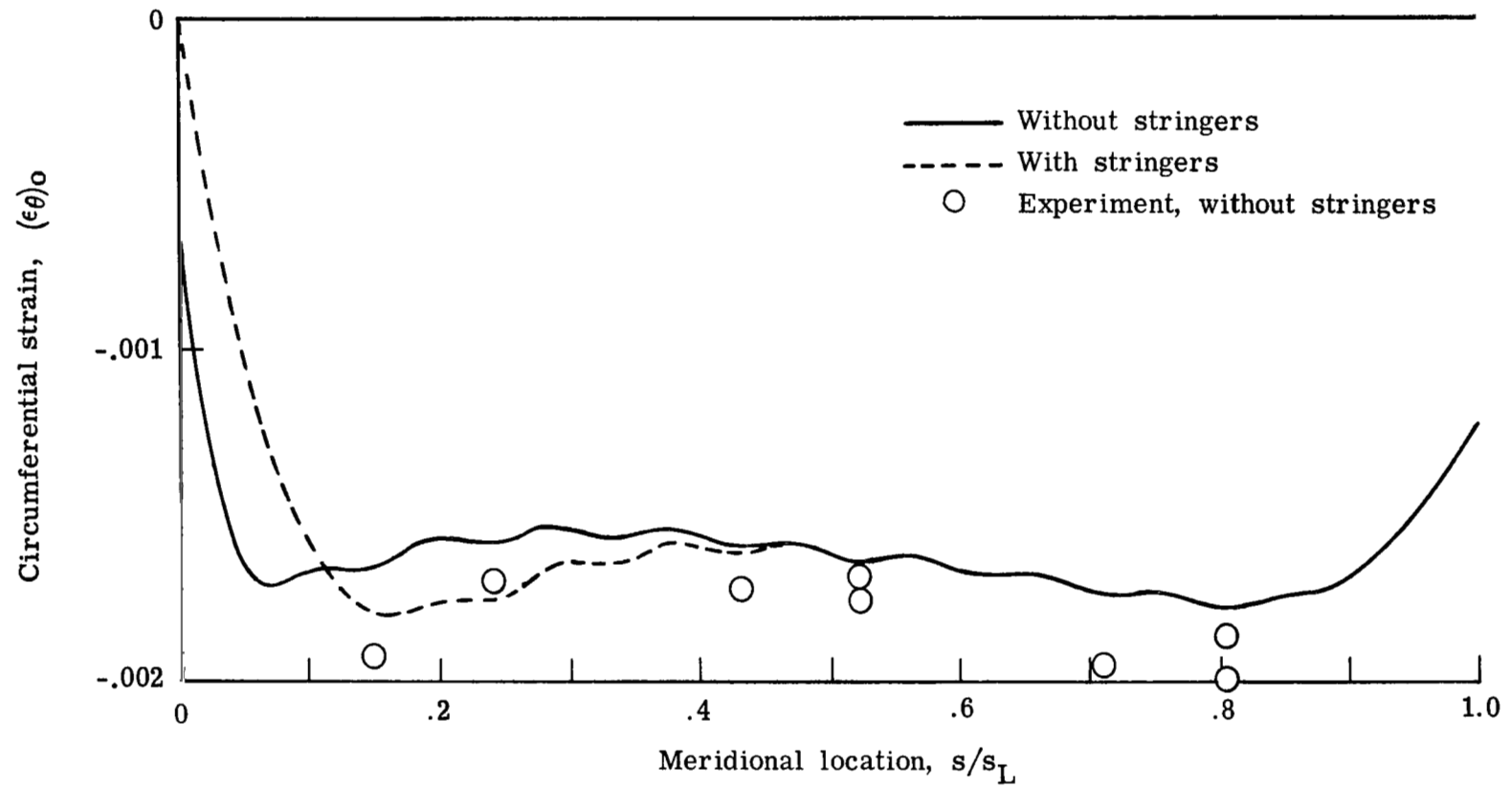
(a) Outside surface.

Figure 5.- Variation of analytical meridional strain with meridional location at 20.5 kN/m^2 external pressure.



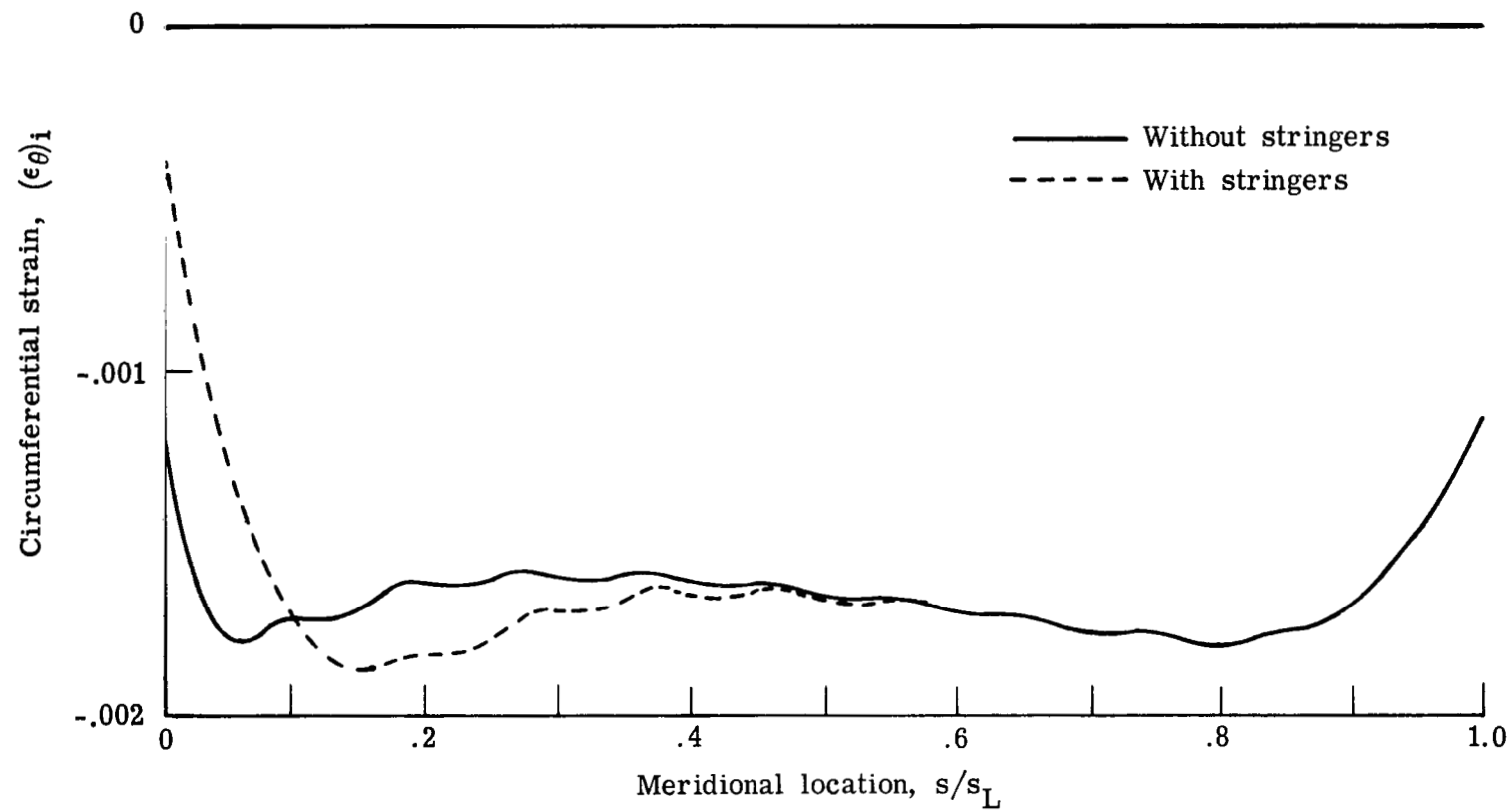
(b) Inside surface.

Figure 5.- Concluded.



(a) Outside surface.

Figure 6.- Variation of circumferential strain with meridional location at 20.5 kN/m^2 external pressure.



(b) Inside surface.

Figure 6.- Concluded.

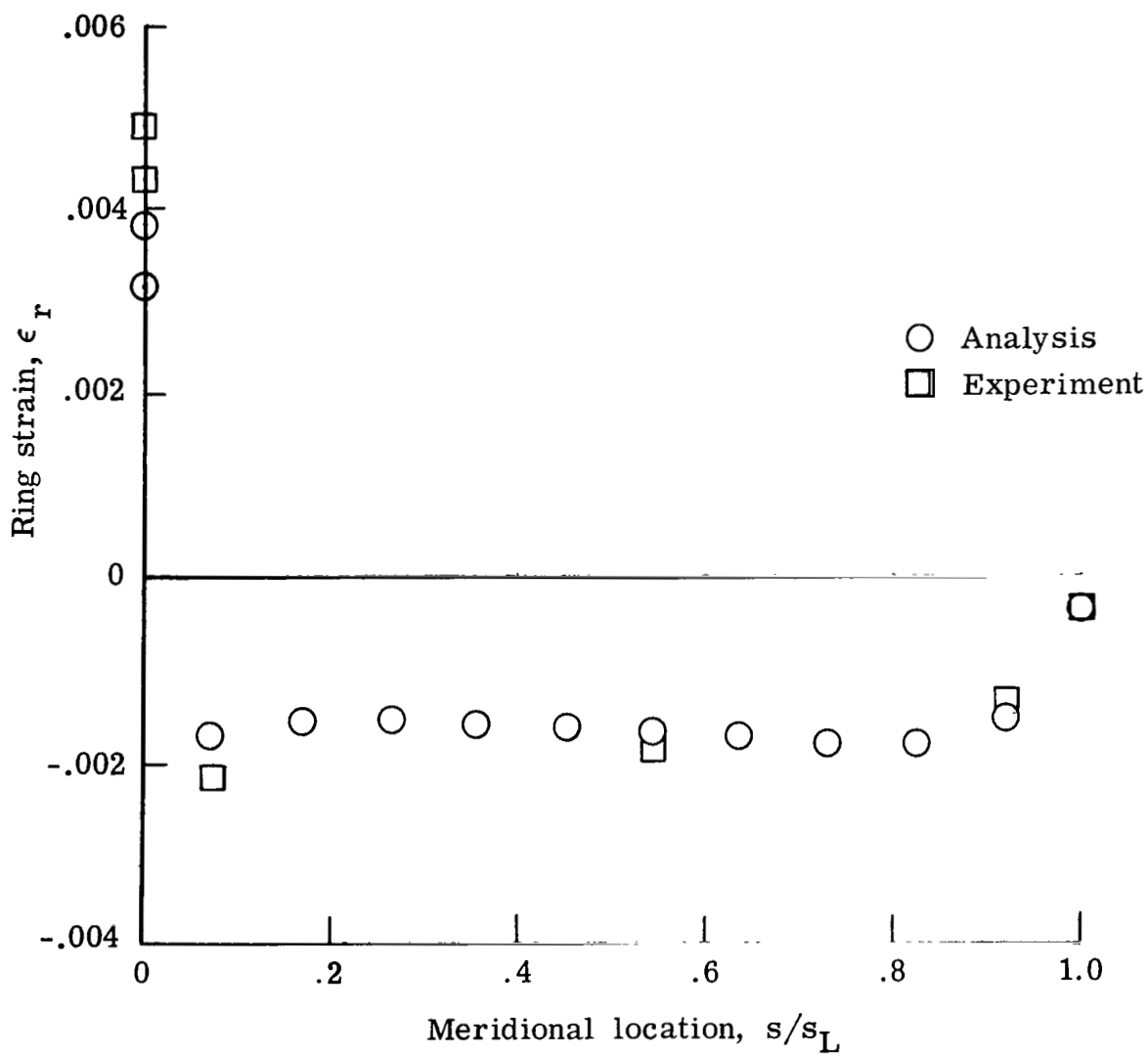


Figure 7.- Ring-circumferential-strain comparison of nonlinear analysis with experiment at 20.5 kN/m² external pressure.

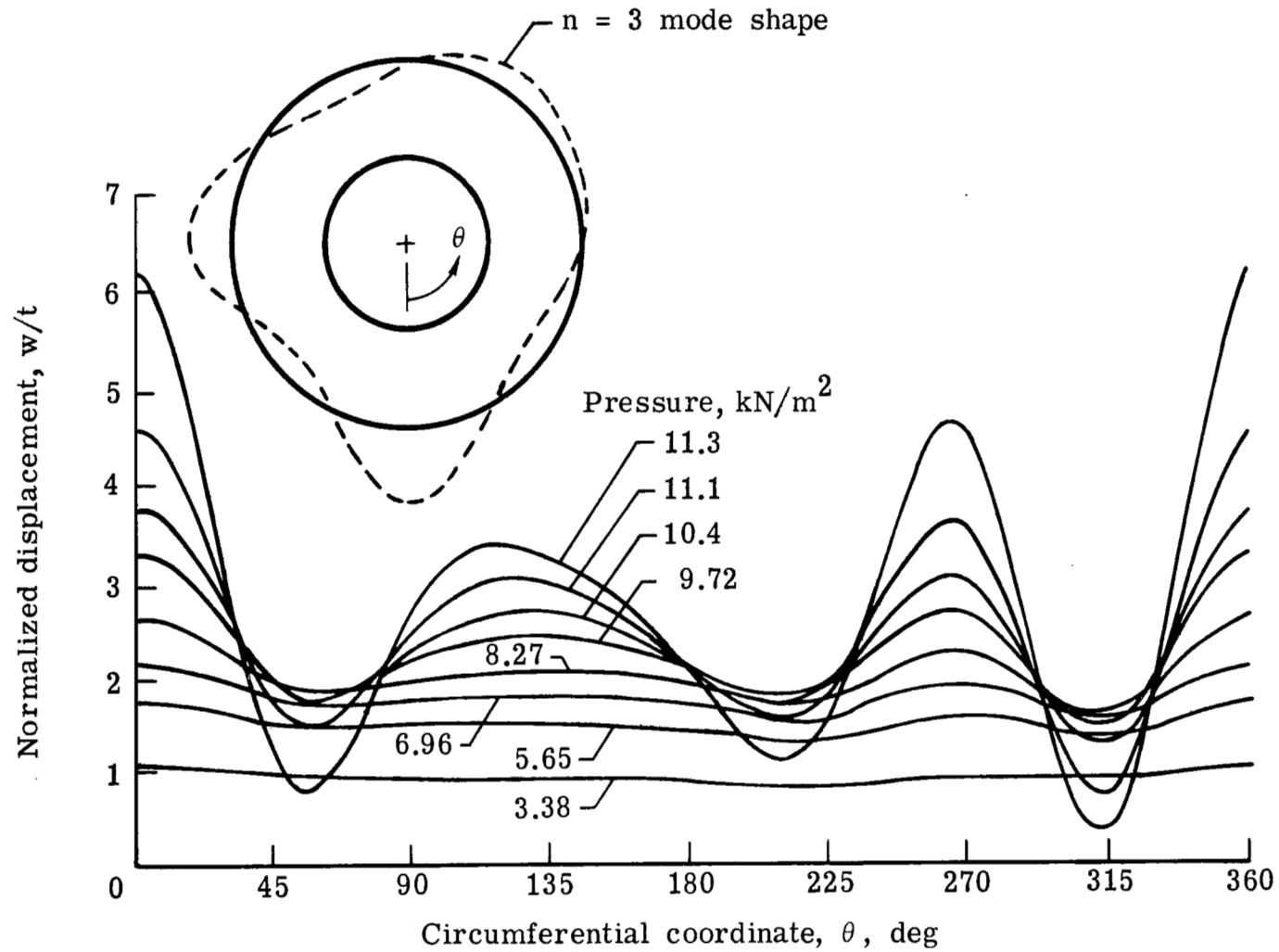


Figure 8.- Variation of measured normalized displacement with circumferential coordinate for selected values of applied external pressure. Case 3; inextensional mode.

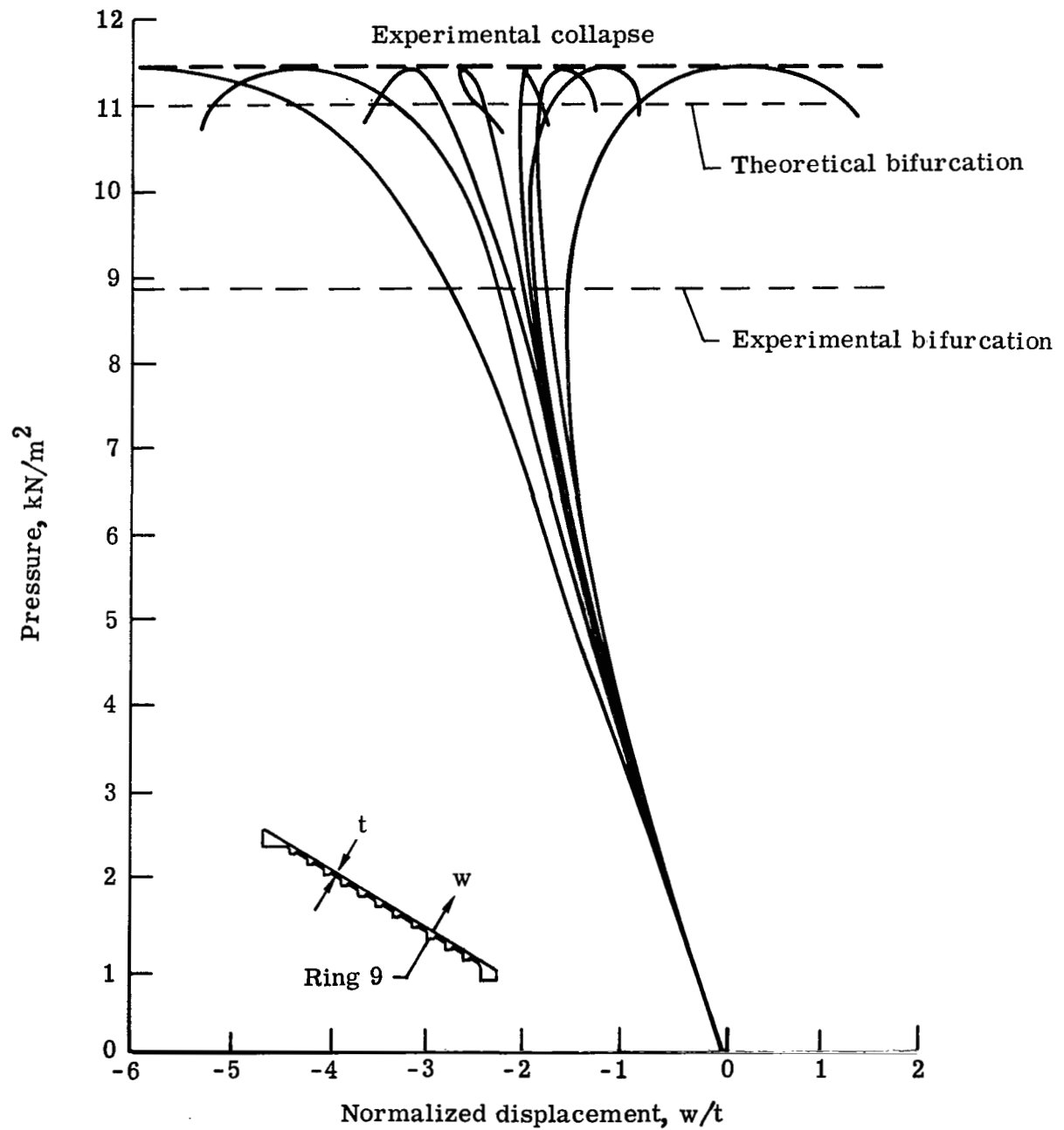


Figure 9.- Variation of normalized displacement at ring 9 with external pressure, measured at eight circumferential stations. Case 3; inextensional mode.

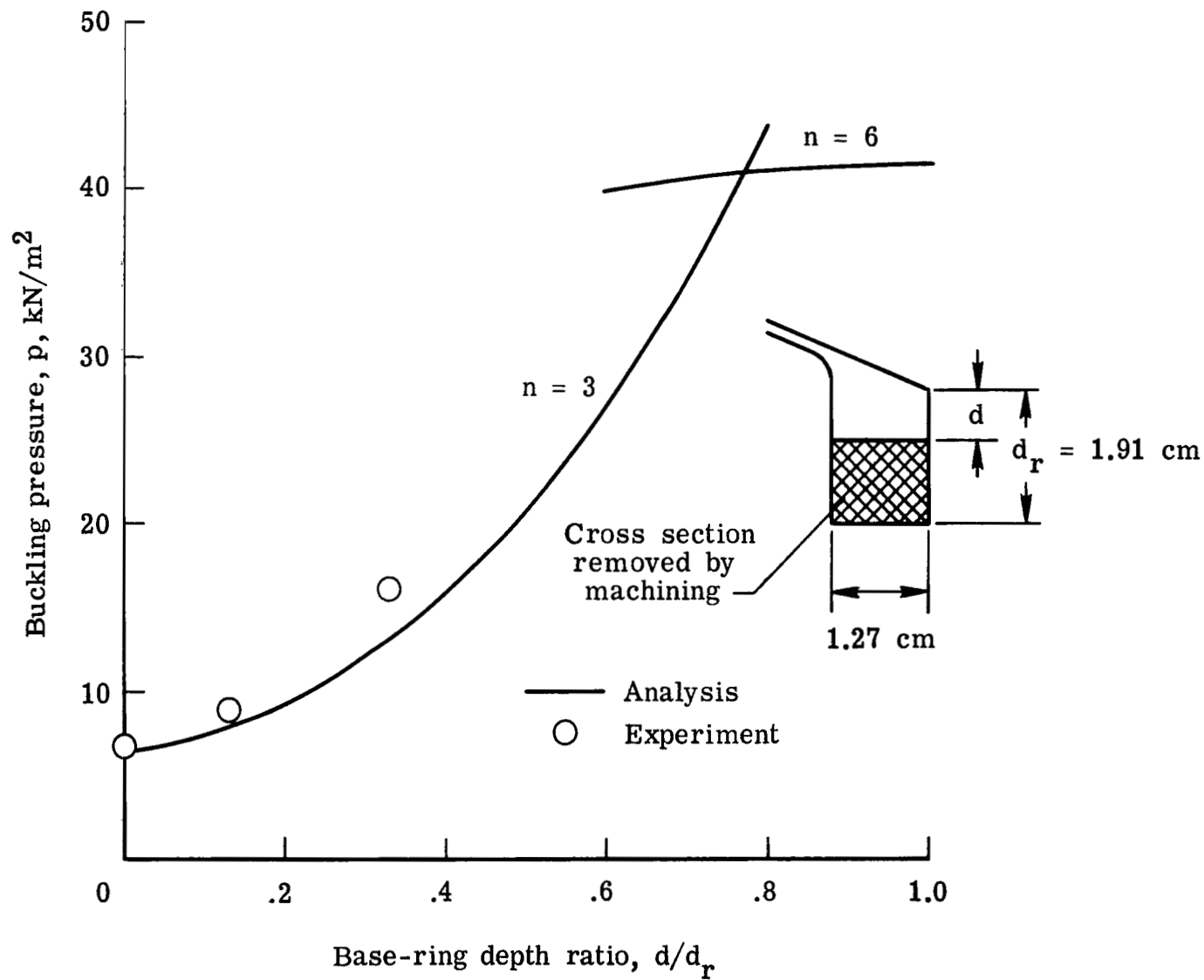


Figure 10.- Variation of buckling pressure from a nonlinear prebuckling stress state with normalized base-ring depth ratio without stringers.

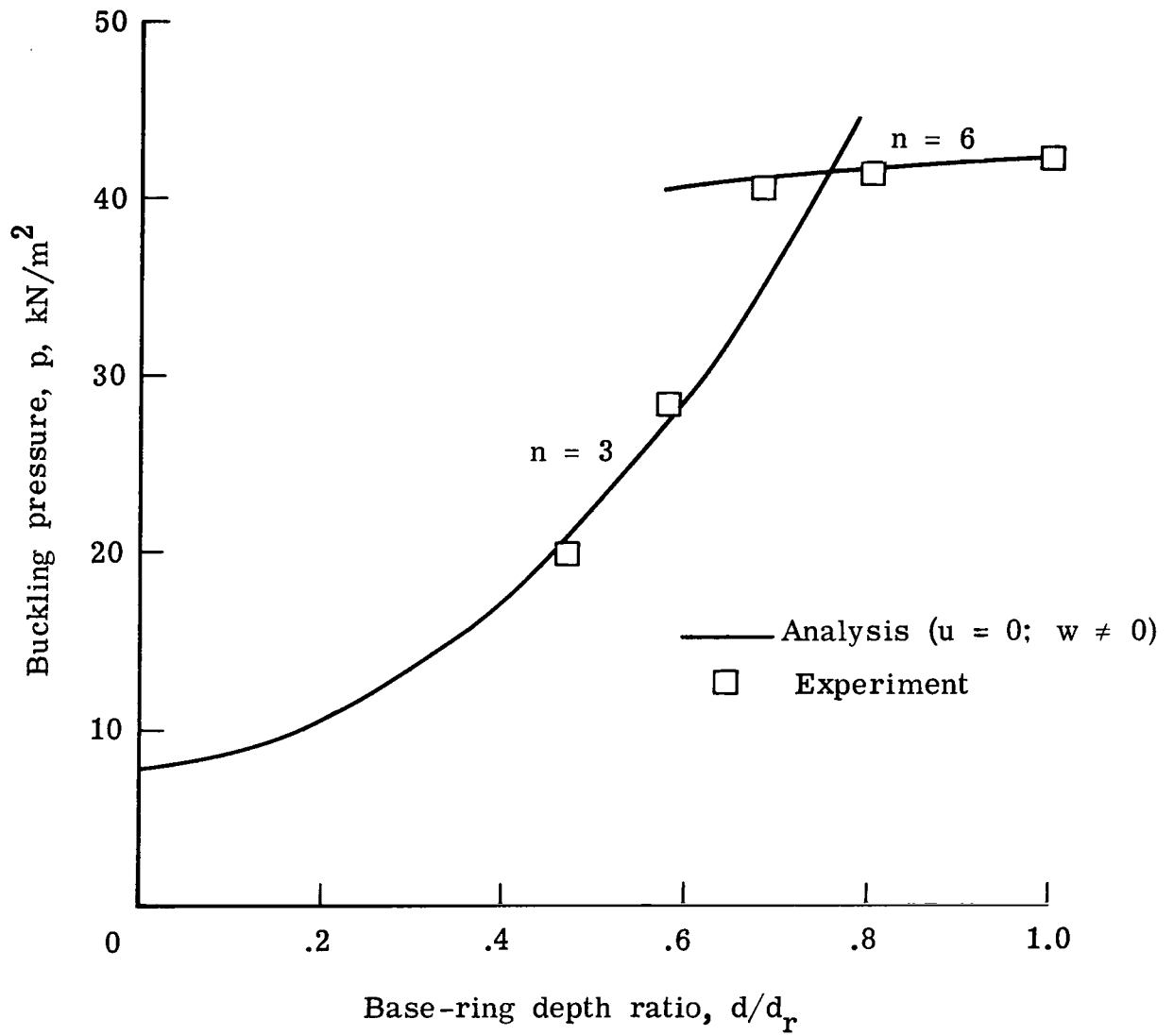
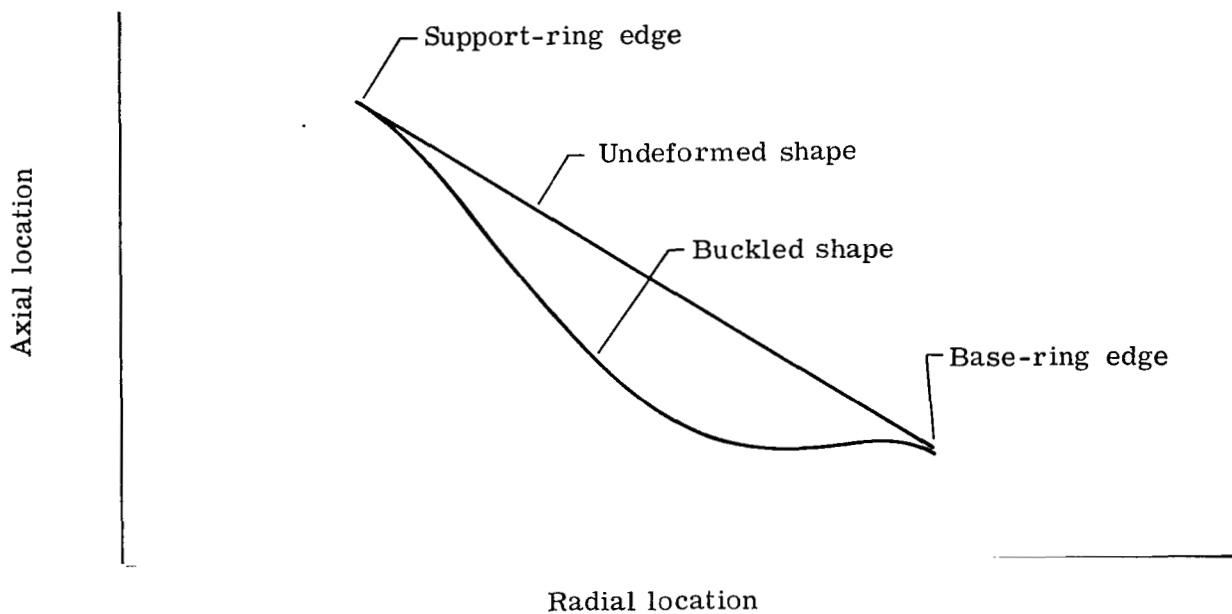
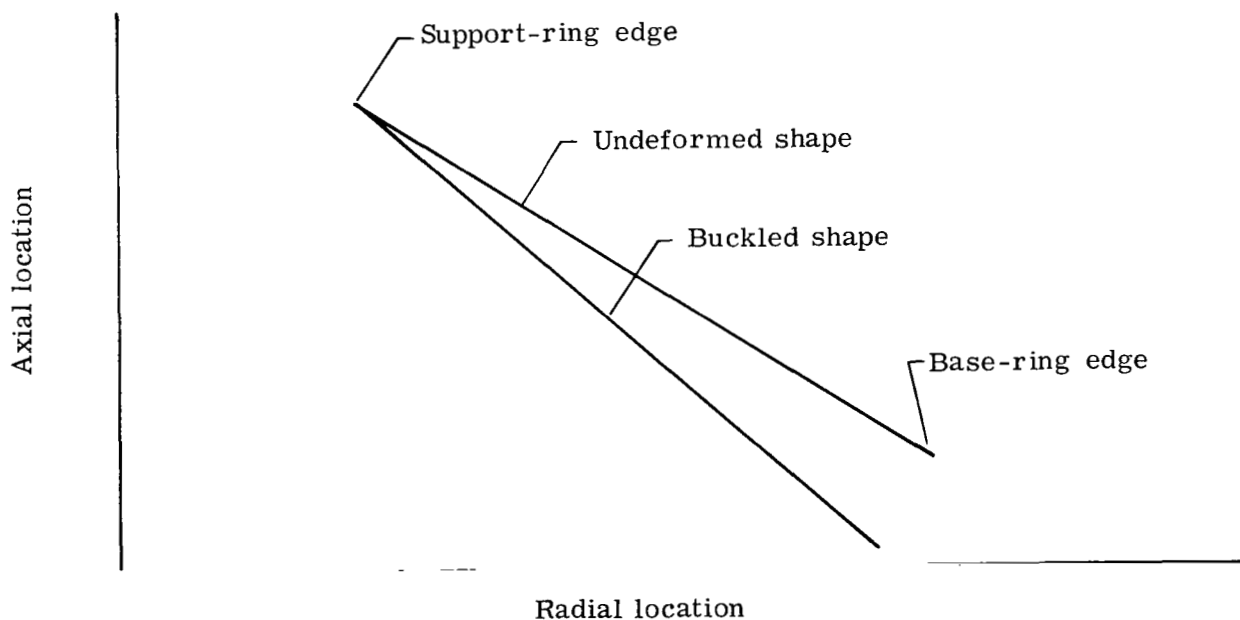


Figure 11.- Variation of buckling pressure from a nonlinear prebuckling stress state with normalized base-ring depth ratio with stringers.



(a) Extensional mode; $n \geq 4$.



(b) Inextensional mode; $n = 2$ or 3 .

Figure 12.- Buckling mode shapes representative of two different types of buckling behavior.

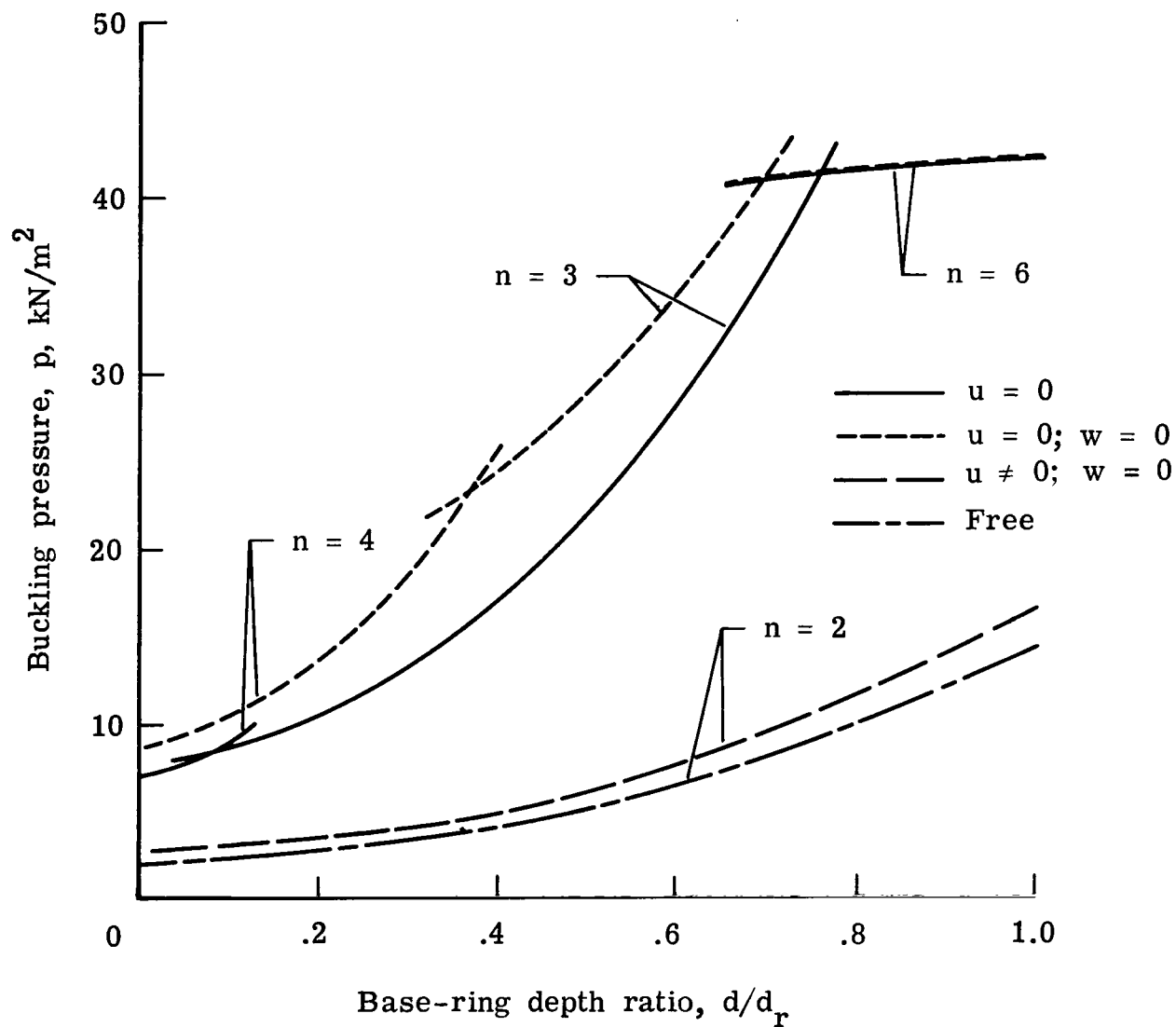


Figure 13.- Buckling pressure from a linear prebuckling stress-state analysis for cone F with various axial and radial buckling boundary conditions at support edge.

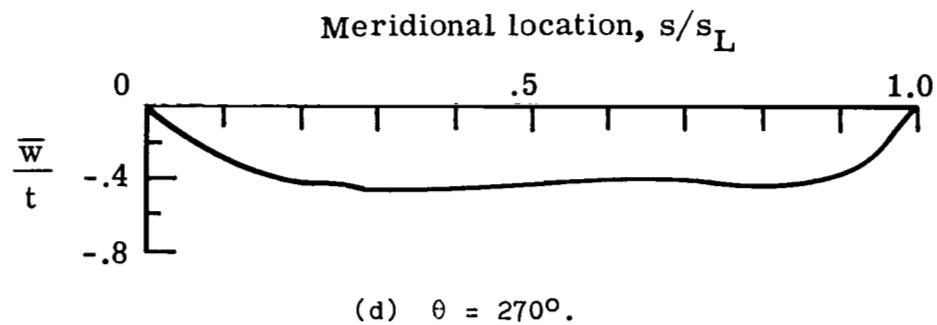
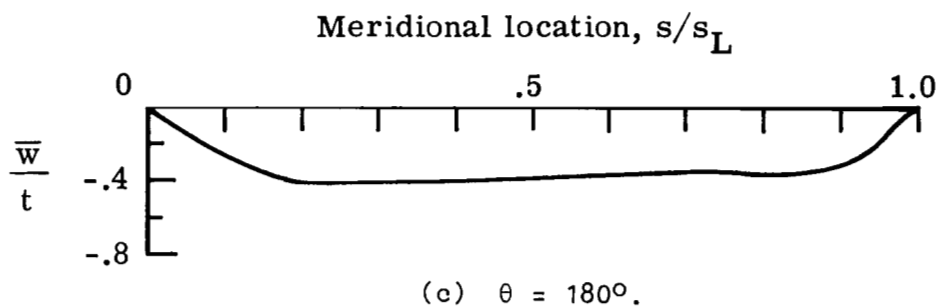
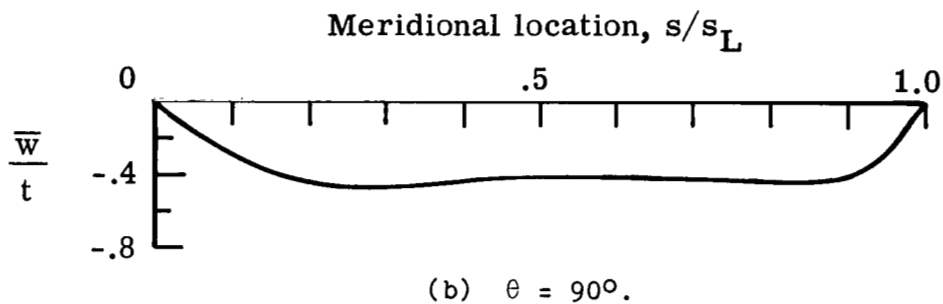
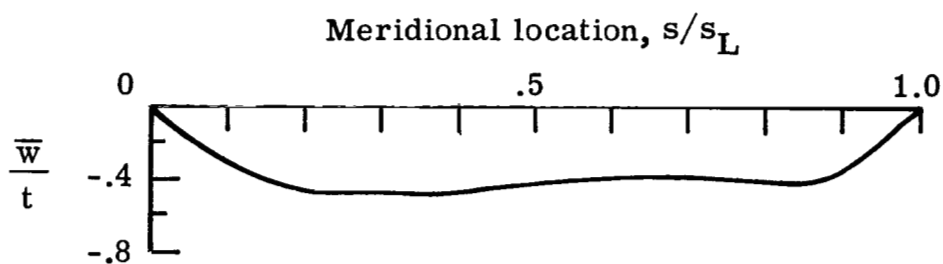
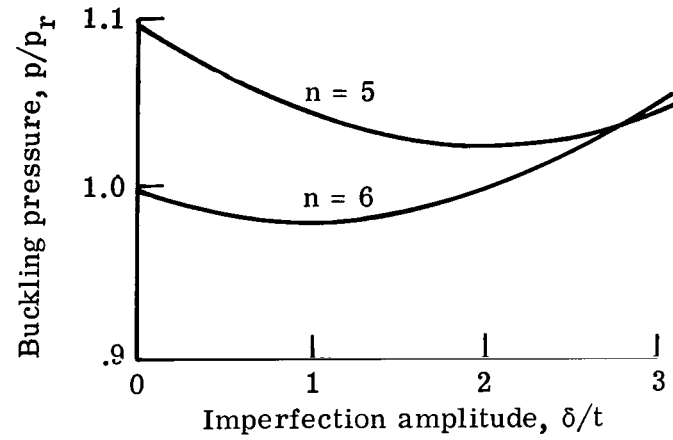
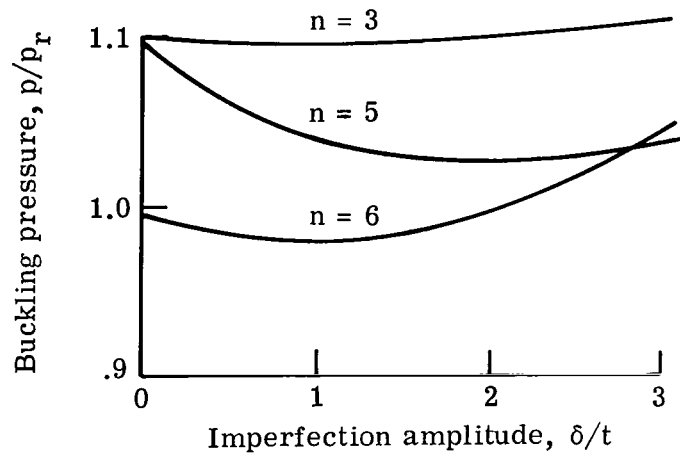


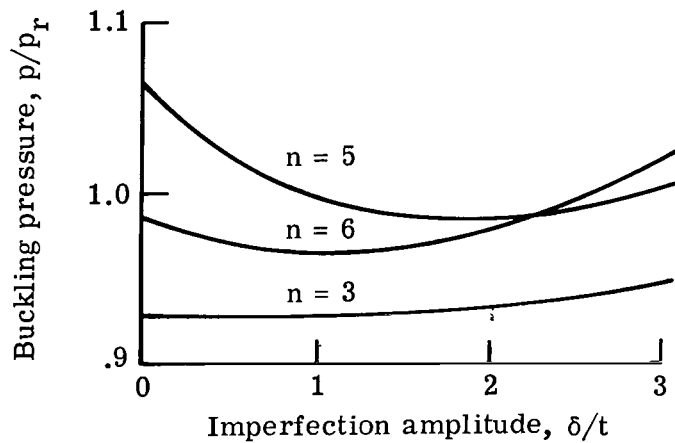
Figure 14.- Meridional imperfections for conical shell specimen C surveyed at four circumferential positions 90° apart.



(a) $d/d_r = 0.8$.



(b) $d/d_r = 0.75$.



(c) $d/d_r = 0.67$.

Figure 15.- Buckling pressures near transition base-ring depth ratio showing sensitivity of various modes to sinusoidal imperfections of amplitude.

1. Report No. NASA TP-1079		2. Government Accession No.		3. Recipient's Catalog No.	
4. Title and Subtitle EFFECT OF END-RING STIFFNESS ON BUCKLING OF PRESSURE-LOADED STIFFENED CONICAL SHELLS				5. Report Date December 1977	
				6. Performing Organization Code	
7. Author(s) Randall C. Davis and Jerry G. Williams				8. Performing Organization Report No. L-11915	
9. Performing Organization Name and Address NASA Langley Research Center Hampton, VA 23665				10. Work Unit No. 506-17-25-01	
				11. Contract or Grant No.	
12. Sponsoring Agency Name and Address National Aeronautics and Space Administration Washington, DC 20546				13. Type of Report and Period Covered Technical Paper	
				14. Sponsoring Agency Code	
15. Supplementary Notes					
16. Abstract Buckling studies were conducted on truncated 120° conical shells having large end rings and many interior reinforcing rings that are typical of aeroshells used as spacecraft decelerators. Changes in base-end-ring stiffness were accomplished by simply machining away a portion of the base ring between successive buckling tests. Initial imperfection measurements from the test cones were included in the analytical model.					
17. Key Words (Suggested by Author(s)) Truncated cone Shells Buckling External pressure Cast-epoxy model Imperfections				18. Distribution Statement Unclassified - Unlimited Subject Category 39	
19. Security Classif. (of this report) Unclassified	20. Security Classif. (of this page) Unclassified	21. No. of Pages 30	22. Price* \$4.50		

National Aeronautics and
Space Administration

THIRD-CLASS BULK RATE

Postage and Fees Paid
National Aeronautics and
Space Administration
NASA-451



Washington, D.C.
20546

Official Business

Penalty for Private Use, \$300

4 1 1U,D, 113077 S00903DS
DEPT OF THE AIR FORCE
AF WEAPONS LABORATORY
ATTN: TECHNICAL LIBRARY (SUL)
KIRTLAND AFB NM 87117

NASA

POSTMASTER:

If Undeliverable (Section 158
Postal Manual) Do Not Return

S